Journal of Thermal Analysis and Calorimetry
https://doi.org/10.1007/s10973-017-6865-4

Experimental and theoretical investigation on the effects of lower concentration CeO_2/water nanofluid in flat-plate solar collector

P. Michael Joseph Stalin[1] · T. V. Arjunan[2] · M. M. Matheswaran[3] · N. Sadanandam[2]

Received: 19 April 2017 / Accepted: 29 November 2017

Abstract

Heat transfer characteristics of solar flat-plate collectors are improved by applying various nanofluids as the heat transfer media nowadays. In the present work, the theoretical and experimental analysis was performed for a flat-plate solar collector operating with water and CeO_2/water nanofluid as the working fluids. The flat-plate solar water heater with 100 L per day capacity along with ladder-type heat exchanger having collector area of 2 m^2 is fabricated for the experimental study. The average particle size and volume fraction of nanofluids were considered as 25 nm and 0.01%, respectively. The flow rate of water and nanofluid was varied from 1 to 3 lpm, and the efficiency was calculated as per ASHRAE standards. Due to the enhanced thermophysical properties of the nanofluid, it gives better performance and results showing that the maximum efficiency of solar water heater with CeO_2/water nanofluid is 78.2%, which is 21.5% higher when compared with the water as base fluid. Also a correlation was developed for predicting the outlet temperature of a flat-plate collector. The maximum collector efficiency of nanofluid was obtained at the optimum mass flow rate of 2 lpm in experimental study. The developed mathematical model was reasonably matching the experimental results with the error of ± 7.5%.

Keywords Flat plate · Solar water heater · Nanofluid · CeO_2 · Heat exchanger

List of symbols

A_c	Surface area of solar collector (m^2)
C_p	Specific heat at constant pressure (J kg^{-1} K^{-1})
G_T	Global solar radiation (W m^{-2})
$\dot{m}$	Mass flow rate of fluid flow (kg s^{-1})
T_a	Ambient temperature (°C)
T_i	Inlet fluid temperature of solar collector (°C)
T_o	Outlet fluid temperature of solar collector (°C)
Q_u	Rate of useful energy gained (W)
F_R	Heat removal factor
Q	Flow rate (lpm)
S	Received solar radiation (W m^{-2})
μ	Viscosity (kg m^{-1} s^{-1})
K	Thermal conductivity (W m^{-1} K^{-1})
ρ	Density (kg m^{-3})
N_g	Number of glass covers
T_p	Mean temperature of the plate (°C)
U_L	Overall heat loss coefficient (W m^{-2} K^{-1})
h_{cca}	Convective heat transfer coefficient between cover and air (W $m^{-2}K^{-1}$)
h_{rca}	Radiative heat transfer coefficient between cover and air (W m^{-2} K^{-1})
h_{cpc}	Convective heat transfer coefficient between plate and cover (W m^{-2} K^{-1})
h_{rpc}	Radiative heat transfer coefficient between plate and cover (W m^{-2} K^{-1})

Greek symbols

α	Transmittance of glass cover
τ	Absorptance of plate

Subscripts

ave	average
nf	nanofluid
bf	base fluids
np	nanoparticle
exp	experimental
theo	theoretical

✉ P. Michael Joseph Stalin
p_mjs1977@yahoo.co.in

[1] Ranganathan Engineering College, Coimbatore641109, India

[2] Coimbatore Institute of Engineering and Technology, Coimbatore 641109, India

[3] Jansons Institute of Technology, Coimbatore 641659, India

Published online: 11 December 2017

Introduction

Non-conventional energy sources play a vital role in the current world economy because these energies are clean, safe and sustainable. Solar energy is one of the renewable energies which are unlimited free source of energy that can be harnessed in the future energy needs without affecting the atmosphere. The critical problem in the solar water heater is efficient use of solar thermal utilization. It is possible that the efficiency can be improved by optimizing the structure of solar collector or developing a new type of working fluid. Currently, water is being used widely as a working medium in conventional flat-plate solar water heating systems. But the thermal characteristics of water are so poor that the performance enhancement cannot be improved to satisfactory level.

Sujit Kumar Verma and Arun Kumar Tiwari analysed the various research works using nanoparticles mixed in base fluids in solar collectors carried out by many researchers during last one decade and mentioned that nanofluids have great potential for thermal systems [1]. At present, more researchers have been involved to enrich the performance of solar water heaters by using the different type of nanofluids as working medium [2]. Fuskele et al. [3] have reviewed the various methods of preparing nanofluids and their synthesis which were carried out by many researchers during last one decade. They have revealed that most of researchers have prepared metal oxide nanofluids by two-step process as it gives more stability during long run. Also they have expressed that hybrid nanofluids have shown improvement in their thermophysical properties. Generally the thermal conductivity of the metals when they are in solid phase is higher than that of fluid phase [4]. In order to increase the outlet temperature and performance, high thermal property nanoparticles is mixed with the primary working fluid to form nanofluids, thereby improving the effective thermal conductivity of the primary fluid [5, 6]. Srivastva et al. [7] have reviewed research works carried out by various researchers and revealed that most of them formulate the heat transfer fluids by evaluating their thermophysical properties of viscosity and thermal conductivity but at lower temperature ranges only with the help of different equipments. Also they found that most of the researches are directed at development of high-performing nanofluids. The thermal efficiency of solar collector using nanofluids depends on several thermophysical properties of nanoparticle such as shape, pH, particle diameter, thermal conductivity, viscosity, volume concentration and specific heat. The use of nanoparticle results in higher thermal efficiency due to the efficient absorption of thermal energy and enhanced radioactive properties of nanofluids [8]. Metal oxide nanoparticles release metal ions in aquatic systems undergoing physical–chemical and biological processes. Particle shape, size, coating, salinity, composition ions, UV irradiation and the presence of contaminants are all factors affecting transformation processes of metal oxide nanoparticles in heterogeneous systems [9].

The effect of copper nanoparticle on a flat-plate solar collector with various volume flow rates and weight fractions was studied by Zamzamian [10] and observed that maximum efficiency has been achieved at 0.3 mass% Cu nanofluid at 1.5 lpm. In another investigation, it was seen that the thermal performance of solar water heater using CuO/water nanofluid prepared with low volume concentration of 0.05% has improved to the tune of 6.3% [11]. Moghadam et al. [12] have investigated experimentally to study the effect of CuO/water nanofluid having 40-nm particle size and found that nanofluid having 0.4% volume fraction with 1 kg/min has increased the collector efficiency up to 21.8% when compared with its base fluid. He et al. [13] have studied the effect of Cu–H_2O nanofluids having 25-nm particle size with 0.1 and 0.2 mass%, respectively, as the absorbing medium and revealed that the efficiency of solar collector was enhanced by 23.83% for 0.1 mass%. Menbari et al. [14] have studied, both analytically and experimentally, the effect of CuO/water nanofluid on the performance of a direct absorption parabolic collector. The results have shown that the thermal efficiency of the system could be improved from 18% to 52% by increasing volume fraction of nanoparticle from 0.002% to 0.008%. Tooraj et al. [15] have studied the performance of flat-plate solar water heater experimentally using 15-nm size nanoparticles with 0.2% weight fraction of Al_2O_3/water nanofluid with the help of Triton X100 surfactant and observed that 28.3% enhancement in thermal efficiency. In another experiment carried out by Gangadevi et al. [16], they found that low volume fraction nanofluids have shown better results when experimented with Al_2O_3 and TiO_2 nanofluids. An experimental study was performed by Raei et al. [17] to investigate the effects of γ-Al_2O_3/water nanofluid on the hydrodynamics and convective heat transfer of a counterflow double-tube heat exchanger at three different flow rates 7, 9 and 11 lpm with 0.05 and 0.15% of nanoparticle volume concentrations. They found that the greatest enhancement in the heat transfer coefficient and the friction factor was obtained at 0.15% volume concentration of nanoparticles. Gupta et al. [18] carried out an experimental study to investigate the effect of 20-nm size of Al_2O_3–H_2O nanofluid in direct absorption solar collector with 0.005% volume fraction at three flow rates and found that enhancement in the

efficiency of the collector reached up to 8.1% with the volume flow rate of 1.5 lpm. In another experimental investigation, Colangelo et al. [19] used Al_2O_3/distilled water nanofluid at 3.0% volume concentration in a modified flat-panel solar thermal collector and achieved an increase in thermal efficiency about 11.7% compared to water as base fluid. In the same manner, Mahian et al. [20] conducted a theoretical study on the performance of Al_2O_3/water nanofluid in a flat-plate solar collector for different particle sizes and volume concentration. Verma et al. [21] have studied the impact of mass flow rate and particle volume fraction using MgO nanofluid on the efficiency of the collector experimentally and observed an efficiency enhancement of about 9.34% in comparison with water as working fluid for 0.75% particle volume fraction at 1.5 lpm volume flow rate. Meibodi et al. [22] have studied the entropy generation analysis of a flat-plate solar collector using SiO_2/ethylene glycol–water nanofluids as base fluids and revealed that entropy generation parameter reduces with increase in nanofluid concentration. Also it was found that exergy efficiency increased for 1 lpm mass flow rate and decreased for further increase in mass flow rate.

It has been observed that for graphene oxide nanofluid with mass concentration 0.02 and a flow rate of 0.0167 kg s^{-1}, the improvement in the collector efficiency was 7.3% over that of the distilled water [23]. Improvement in thermal conductivity has been achieved up to 32% by mixing only 150 ppm functionalized carbon nanotubes to water and it has increased the overall efficiency of direct absorption solar collectors [24]. Natarajan and Sathish [25] have investigated that the use of nanoparticle and carbon nanotube enhanced the efficiency of solar water heater due to the enhanced absorption of solar energy. Since Al_2O_3 and carbon nanotubes have superior thermal conductivity in addition to low density, many research works are being carried out at present. Estelle et al. [26] investigated the thermophysical properties and convective heat transfer performance of CNT at 45 °C in a coaxial heat exchanger working in concurrent flow considering water–ethylene glycol as base fluid and lignin as surfactant. The results have shown that the presence of ethylene glycol plus water as base fluid and higher nanoparticle content can be suitable for the best heat transfer applications. Delfani et al. [27] have studied the effect of residential-type direct absorption solar collector using MWCNT nanofluid with the various flow rates and 100 ppm volume fraction. The results show that the highest collector efficiency was achieved at the flow rate of 90 LPH and it was about 29% more than that of the base fluid at same flow rate. Pandey et al. [28] evaluated the thermal performance of direct flow evacuated tube collector-based solar water heating system by utilizing the concept of energy and exergy analyses. They varied the volume flow rates from 10 LPH to 30 LPH in steps of 5 LPH. They found that the performance was maximum for 15 LPH and minimum for 30 LPH. Also they revealed that energy efficiency was higher than exergy efficiency for all the volume flow rates. Many researchers tried to establish various theories in order to understand the behaviour of nanoparticles through various parameters such as heat transfer coefficient, particle size and extinction coefficient. [29]. Brownian motion and thermophoresis were also developed [30] for the above theories. The efficiency, cost, savings, size, environmental impact and payback period of a flat-plate solar collector were estimated for various nanofluids [31] and concluded that nanofluid decreases the carbon emission and embodied energy by approximately 3 and 9%, respectively [32]. Hama et al. [33] have studied the overall heat transfer coefficient of various nanofluids Al_2O_3, TiO_2, Fe_2O_3, CuO, CNT and SiO_2, with the limitation of the dispersion stability and found that the nanofluids Fe_2O_3 and CuO were superior to other nanofluids with respect to the enhancement of the overall heat transfer coefficient. Koa et al. [34] have synthesized CeO_2-covered nanofiber through amine group immobilization onto an electro-spun polyacrylonitrile nanofiber. It was found that CeO_2-covered nanofiber played an effective role in lowering the phosphate ions in an aqueous solution by the oxidation, reduction and ion-exchange processes in lakes and rivers to prevent water eutrophication.

Even though, in the past many research works have been carried out with various nanofluids by considering concentration from 0.05 to 4%, most of them have concluded that optimum efficiency was obtained in the lower concentration for various reasons. The CeO_2 is an economically feasible commercial nanoparticle when compared to the cost of CuO, TiO_2, SiO_2 etc. Since CeO_2/water is a chemically inert nanofluid with copper material and has superior thermal conductivity [35] in addition to low specific heat, it has been considered as working fluid with lower volume concentration of 0.01% in the present study. The main objective of this study is to find the effect of volume flow rate with lower volume concentration of CeO_2/water nanofluid on the performance of flat-plate solar collector both experimentally and theoretically.

Solar water heating system

Development of experimental setup

The schematic diagram of the solar water heating system is shown in Fig. 1. The experimental setup consists of flat-plate solar collector, storage tank and ladder-type heat exchanger. The dimensions of the solar collector are 2 m long, 1 m wide and 0.15 m high, and the area of the

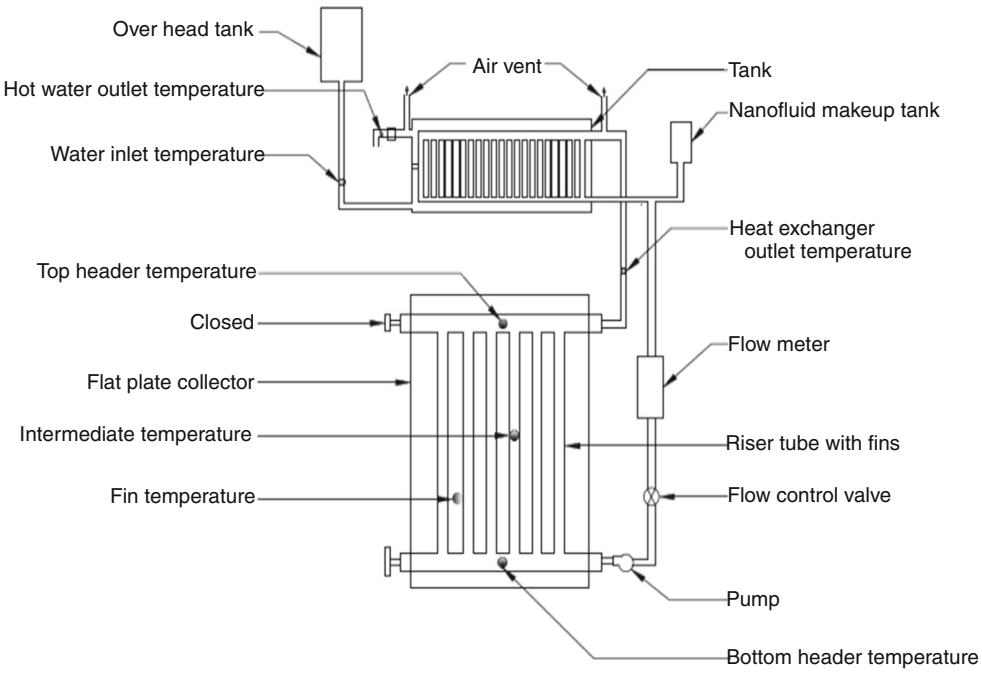

Fig. 1 Schematic diagram of the experimental setup

collector is 2 m^2. A copper sheet of 0.45 mm thick is used as the absorber plate, and a transparent glass of 4 mm thick is used to cover the collector in order to reduce the loss of radiation. The absorber plate is painted with black to absorb maximum solar radiation. The gap between the absorber plate and glass cover is 30 mm. The collector bottom and side are insulated using glass wool with a thickness of 50 and 25 mm, respectively, to reduce the heat loss by convection. The storage tank consists of an inner tank and an outer tank with 100-mm gap between two tanks, which are filled by glass wool in order to reduce the heat losses from the hot water to atmosphere. The solar collector which consists of nine parallel tubes (risers) of 10 mm diameter on the backside of the absorber plate is connected at the top and bottom by headers to provide homogeneous flow distribution and static pressure at inlet and outlet section. The photographic view of the experimental setup shown in Fig. 2 was fabricated and installed at Solar Energy Research Centre, Coimbatore Institute of Engineering and Technology. The experimental investigations were conducted with various parameters under the meteorological conditions of Coimbatore, India (latitude of 11.0183°N; longitude of 76.9725°E) during the months of March and April 2016. The experiments were conducted day to day, and based on the solar radiation similarity pattern, the data were selected and presented in this study to get concurrent results. The specifications of the solar collector are given in Table 1. The experimental setup is fabricated with suitable and reliable measuring instruments in order to study the performance of flat-plate solar water heating system. Before conducting the experiments, the

Fig. 2 Photographic view of the experimental setup

nanofluid of 8.5 L was prepared and filled into heat exchanger circuit with the help of makeup tank. The storage tank was filled with water so that heat can be absorbed from the heat exchanger in forced circulation. An electrical pump was employed to pump the nanofluids for circulation in the heat exchanger. A flow control valve and rotameter were used to control and measure the flow rate of working fluid, respectively. The experiments were conducted as per ASHRAE standards, and the analysis was performed based on real and consistent meteorological data recorded every 30 min of interval from the period of 9:00–16:00 h during

Table 1 Specifications of flat-plate solar collector for the experimental study

Sl. no.	Description	Dimension
1	Length of the collector	2000 mm
2	Width of the collector	1000 mm
4	Collector tilt angle	15°
5	Thickness of back insulation	50 mm
6	Thickness of edge insulation	25 mm
7	Absorber plate thickness	0.454 mm
8	Thermal conductivity of the absorber plate	386 Wm^{-1} K^{-1}
9	Emissivity of absorber plate	0.95
11	Thickness of the glass cover	4 mm
12	Emissivity of glass cover	0.88
13	Tube spacing between risers (9 nos)	95 mm
14	Inner diameter of the riser pipe	9.5 mm
15	Outer diameter of the riser pipe	10 mm
16	Header pipe diameter	25 mm

the investigation. Thermocouples of K-type having an accuracy of ± 0.5 °C have been placed at eight locations of the experimental setup consisting of heat exchanger, solar collector and storage tank for measuring the temperatures of water flowing through the system and connected with an eight channel digital temperature indicator having a resolution of ± 0.1 °C. Solar power meter (Make—TES Electrical electronics, Model-1333, Range − 1 to 2000 W m^{-2}) with an accuracy ± 10 W m^{-2} is used to measure solar intensity.

Preparation of nanofluid

Commercial spherical shape cerium oxide powders with 99.5% of purity with an average diameter of 25 nm mixed with water as a base fluid was used in this study. The required quantity of working fluids to be circulated through the system is 8.5 L. For preparing a CeO_2/water nanofluid with 0.01% volume fraction, the quantity of nanoparticles was estimated to be 0.713 g. Using a magnetic stirrer, the required amount of CeO_2 nanoparticles was slowly added with water while maintaining constant stirring for about half an hour initially. For obtaining a homogeneous mixture, once again the prepared solution was sonicated continuously using ultrasonic vibrator for another 30 min approximately with a frequency range from 15 to 100 Hz, thereby breaking down the agglomeration of CeO_2 nanoparticles and water. The properties of nanoparticle, base fluid and CeO_2/water nanofluid are indicated in Table 2.

Determination of efficiency

The useful energy gain (Q_u) was determined based on the energy absorbed by the absorber and the energy lost from the absorber by using following Eqs. (1) and (2).

$$Q_u = \dot{m}\, C_p(T_o - T_i) \tag{1}$$

where $\dot{m}$ and C_p denote mass flow rate and heat capacity of fluid and T_o and T_i are the outlet and inlet fluid temperatures, respectively.

$$Q_u = F_R[G_T(\tau\alpha)\ \cdot A_C - U_l A_C(T_i - T_a)] \tag{2}$$

where F_R is heat removal factor, which can be expressed by Eq. (3).

$$F_R = \dot{m}\, C_p(T_i - T_a)\ /\ G_T(\tau\alpha)\ \cdot A_C - U_l\, A_C(T_i - T_a) \tag{3}$$

where "A_C" is surface area of the collector,$(\tau\alpha)$ is the absorptance and transmittance product, G_T is the global solar radiation,U_l is the overall loss coefficient of solar collector and T_a is the ambient temperature. In Eq. (3), actual gain of the collector has been related to the useful energy gain by the collector considering the collector surface temperature as same as that of the fluid inlet temperature. The collector efficiency (η) is used to measure the flat-plate collector performance which may be defined as the ratio of the useful energy gain (Q_u) to the incident solar energy over a particular time period. Moreover, the thermal efficiency (η) can be obtained by dividing Q_u by the energy input ($A_C \cdot G_T$) as in Eq. (4)

$$\eta = F_R[G_T(\tau\alpha)\ \cdot A_C - U_l A_C(T_i - T_a)]\ /A_C\ G_T \tag{4}$$

Table 2 Properties of the base fluid, cerium oxide nanoparticle and CeO_2/water nanofluid

Sl. no.	Material	Thermal conductivity/ Wm^{-1} K^{-1}	Specific heat/ J kg^{-1} K^{-1}	Viscosity / kg m^{-1} s^{-1}	Density/ kg m^{-3}
1	Water	0.52	4187	0.000620	1000
2	CeO_2	12	460	–	7132
3	CeO_2/water nanofluid (0.01%)	0.681	4044	0.000690	1008

Embodied energy and economic analysis

In order to calculate the embodied energy consumption, the energy consumed for manufacturing of solar collector has been considered. The analysis is done due to the reduction in collector area which is the functional unit that influences the overall weight and embodied energy of the collector. By considering the thermal performance of the solar collector, the reduction in the size of collector's area can be estimated by

$$A_C = \dot{m}\, C_p(T_o - T_i) \,/\, G_T\eta \tag{5}$$

The glass having an embodied energy index of 15.9 MJ kg^{-1} and copper with that of 70.6 MJ kg^{-1} (Otanicar et al. [36]) are the two main materials used in the manufacturing of solar collector with the weight ratio of 20-kg glass and 8-kg copper for a 28-kg solar collector. When the solar collector is operated with CeO_2/water nanofluid, reduction in collector area of the material consumption is also reduced based on which simple cost analysis has been carried out.

Analytical modelling

In theoretical analysis, it has been assumed that all the risers are parallel to each other and the centerlines joining the absorber plate and risers are located in the same line (refer Fig. 3). Performance of the flat-plate solar collector using CeO_2/water nanofluid as the working fluid is considered and compared with results of water as base fluid. For calculating the thermophysical properties of nanofluids, the model given by Xuan et al. [37] is considered which includes the aggregation and Brownian motion of nanoparticles. This model is described as follows

$$\frac{k_{nf}}{k_{bf}} = \frac{k_{np} + 2k_{bf} - 2\varphi\left(k_{bf} - k_{np}\right)}{k_{np} + 2k_{bf} + \varphi\left(k_{bf} - k_{np}\right)} + \frac{\rho_p \varphi C_{pf}}{2k_{bf}}\sqrt{\frac{2K_B T_{ave}}{3\pi d_{np}\mu_{bf}}} \tag{6}$$

in which μ is the viscosity (kg m^{-1} s^{-1}), k is the thermal conductivity (W m^{-1} K^{-1}), T is temperature (K), C_p is heat capacity (J kg^{-1} K^{-1}), ρ is density (kg m^{-3}), ϕ is the volume fraction of nanoparticles and d_{np} is particle size (m). The subscripts of bf, nf and np denote for base fluid, nanofluid and nanoparticle, respectively.

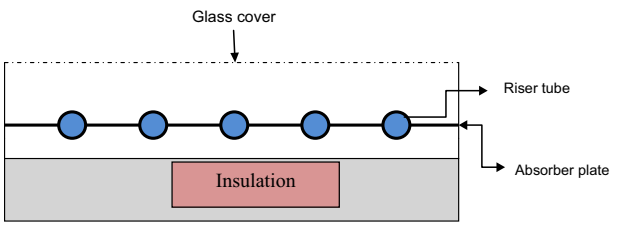

Fig. 3 Schematic layout of flat-plate solar collector

Thermal conductivity of water is computed from the following relation as mentioned in [38]:

$$k_{bf} = 0.6067\left(-1.26523 + 3.704\left(\frac{T_{ave}}{298.15}\right) - 1.43955\left(\frac{T_{ave}}{298.15}\right)^2\right) \tag{7}$$

The average temperature of the fluid is defined as

$$T_{ave} = \frac{T_{in} - T_{out}}{\ln\left(\frac{T_{in}}{T_{out}}\right)} \tag{8}$$

The viscosity is determined by Corcione correlation [39] that can be used for volume fractions up to 10% and is given as under:

$$\mu_{nf} = \frac{\mu_{bf}}{1 - 34.37\left(\frac{d_{np}}{d_{nf}}\right)^{-0.3}\varphi^{1.03}} \tag{9}$$

where d_{nf} is the diameter of the molecule of base liquid and it is defined as

$$d_{nf} = 0.1\left(\frac{6M}{N\pi\rho_{f0}}\right)^{\frac{1}{3}} \tag{10}$$

in which N is Avogadro number, M is the molecular weight of base fluid and ρ_{fo} is the density of base fluid calculated at 293 K. The viscosity of water as a function of temperature is as follows [40]:

$$\mu_{bf} = 2.414 \times 10^{-5} \times 10^{\frac{247}{(T_{ave}-140)}} \tag{11}$$

The density of nanofluid and heat capacity of nanofluid can be calculated using the relations mentioned in [40]:

$$\rho_{nf}\rho_{bf}(1 - \varphi) + \rho_{np}\varphi \tag{12}$$

$$C_{p,nf} = \frac{\rho_{bf}C_{pf}(1 - \varphi) + \rho_{np}C_{np,p}\varphi}{\rho_{nf}} \tag{13}$$

where $C_{p,np}$, Heat capacity of nanoparticle, $C_{p,nf}$, Heat capacity of nanofluid, $C_{p\cdot bf}$, Heat capacity of base fluid and φ, Volume fraction of nanoparticle (%).

First law analysis

During the absorption process of solar radiation, some amount of energy is utilized by the working fluid (Q_u) and the remaining energy is dissipated to the surroundings as ambient. For calculating the efficiency and outlet temperature, the net heat loss to the ambient is to be estimated first. The amount of energy strikes on the absorber plate is given by the relation $S = \eta_o G_t$ where η_o is the optical efficiency of the solar collector. The following equation

gives the relationship between absorbed heat and heat losses.

$$Q_u = A_C\left[S - U_l\left(T_p - T_a\right)\right] \tag{14}$$

where A_c is the surface area of collector (m^2), T_p and T_a are absorber plate temperature and ambient temperature, respectively. Overall heat loss coefficient U_L can be determined as [41] with the assumption that all the heat losses of the collector concentrate to a common sink temperature T_a:

$$U_L = U_t + U_b + U_e \tag{15}$$

where U_t is the heat loss coefficient from the top, U_b is the heat loss coefficient from the bottom and U_e is the heat loss coefficient from the edges of collector. To find U_t, the following correlation can be used as [42]:

$$U_t = \frac{1}{\frac{N_g}{\frac{C}{T_p}\left[\frac{T_p - T_a}{N_g + \tau}\right]^{0.33}} + \frac{1}{h_W}} + \frac{\sigma\left(T_p^2 + T_a^2\right)\left(T_p + T_a\right)}{\frac{1}{\varepsilon_p + 0.05N_g\left(1-\varepsilon_p\right)} + \frac{2N_g + \tau - 1}{\varepsilon_g} - N_g} \tag{16}$$

where N_g is the number of glass covers and it is taken as unity for the current paper, σ is Stefan–Boltzmann constant and ε_p and ε_g are the emissivity of the plate and glass, respectively. The parameter of h_W is the wind heat transfer coefficient and is found by:

$$h_w = \frac{8.6\,V_W^{0.6}}{L^{0.4}} \tag{17}$$

where L and V_w denote the length of collector and wind velocity, respectively. Also the value of h_w is taken as 5 W m^{-2} K^{-1} in case the calculated value of h_w is less than 5 while using the above equations. Incidentally, it also indicates the heat transfer coefficient of still air [42].Moreover, the constants of τ and C are calculated by:

$$\tau = \left(1 - 0.04h_w + 0.0005{h_w}^2\right)\left(1 + 0.091N_g\right) \tag{18}$$

$$C = 365.9\left(1 - 0.00883\beta + 0.0001298\beta^2\right) \tag{19}$$

where β is the collector slope.

The main heat losses occur from the top. To determine the heat losses from the bottom and edges, following equations is used.

Heat loss coefficient from bottom is found by

$$U_b = \frac{1}{\frac{t_b}{k_b} + \frac{1}{h_{b,a}}} \tag{20}$$

and heat loss coefficient from edges is calculated by

$$U_e = \frac{1}{\frac{t_e}{k_e} + \frac{1}{h_{e,a}}}\frac{A_e}{A_c} \tag{21}$$

where k_b, Thermal conductivity of insulator in bottom surface; k_e, Thermal conductivity of insulator in edges; A_e, Surface area of edges; t_b, Thickness of insulator in bottom area; t_e, Thickness of insulator edge.

Moreover, the values of $h_{b,a}$ and $h_{e,a}$ are assumed to be 5 W m^{-2} K^{-1} which represents the convection heat transfer coefficients in the bottom and edges, respectively. An initial value of T_p is assumed for estimating the quantities of U_L and Q_u. Then by using iterative method and the following equations, the value of T_p is corrected.

$$T_p = T_{in} + \frac{Q_u}{A_c F_R U_L}\left(1 - F_R\right) \tag{22}$$

The criterion that is used for the iterative process is given bellow

$$\left|\frac{\left(T_p\right)_{aume} - \left(T_p\right)_{find}}{\left(T_p\right)_{find}}\right| \le 10^{-5} \tag{23}$$

where F_R is heat removal coefficient and is mentioned as [42]:

$$F_R = \frac{\dot{m}C_p}{A_c U_L}\left[1 - \exp\left(-\frac{U_L F' A_c}{\dot{m}C_p}\right)\right] \tag{24}$$

in the above relation F′ is the collector efficiency factor and is as follows [42]:

$$F' = \frac{\frac{1}{U_L}}{W\left[\frac{1}{U_L[D + (W-D)F]} + \frac{1}{\pi D_i h_{fi}}\right]} \tag{25}$$

where D is the outer diameter of risers, D_i is the inner diameter of risers, W is tube spacing and F is standard fin efficiency that is calculated by:

$$F = \frac{\tanh[m(W-D)/2]}{m(W-D)/2} \tag{26}$$

where $m = \sqrt{\frac{U_l}{k_c b_t}}$ in which k_c and b_t are thermal conductivity and thickness of absorber plate, respectively. To obtain the internal heat transfer coefficient (h_{fi}), for laminar flow conditions

$$h_{fi} = \frac{48k_{nf}}{11D_i} \tag{27}$$

Reynolds and Prandtl numbers are defined as:

$$R_e = \frac{4\dot{m}_r}{\pi D_i \mu_{nf}} \tag{28}$$

$$\mathrm{Pr} = \frac{\mu_{nf} C_{p,nf}}{k_{nf}} \tag{29}$$

The Reynolds number is in terms of mass flow rate in any riser ($\dot{m}_r$).

By using MATLAB codes, all the above equations are solved in addition to computing mean temperature of the absorber plate. At the end, the outlet temperature of fluid can be calculated using the following relation

$$T_{out} = T_{in} + \frac{Q_u}{\dot{m} C_p} \tag{30}$$

The thermal efficiency of flat-plate solar collector can be found as [42]:

$$\text{Efficiency} = \frac{Q_u}{A_c G_t} \times 100 \tag{31}$$

Equations for analytical modelling that have been developed above are solved using MATLAB code, and its execution procedure is shown in Fig. 4 The thermal network diagram for flat-plate collector is shown in Fig. 5.

Uncertainty analysis

Uncertainty is required in order to establish the accuracy of the experiments. In any experiment, the measured quantities are subjected to uncertainties or error. The systematic and random errors can be caused by various factors. According to the guidelines of ASME, there will be some errors in the accuracy of instruments due to various reasons such as calibration errors, lack of maintenance of recording instruments, precision of thermocouples, inaccuracy in flow rate measurements and solar intensity measurements and scatter uncertainties. As per Eq. 32 [11], the efficiency of flat-plate solar collector is directly proportional to mass flow rate of nanofluid ($\dot{m}$), temperature difference between the outlet and inlet fluid (ΔT) and specific heat of the nanofluid but inversely proportional to area of solar collector and global solar radiation (G_T).

Hence, the overall uncertainty equation can be followed:

$$\left(\frac{U_{\eta i}}{\eta i}\right)^2 = \left(\frac{U_{\dot{m}}}{\dot{m}}\right)^2 + \left(\frac{U_{G_T}}{G_T}\right)^2 + \left(\frac{U_{\Delta T}}{\Delta T}\right)^2 \tag{32}$$

where U represents uncertainty.

The uncertainty given by the manufacturers of thermocouples and flow meter is ± 0.5 °C and ± 2%, respectively. The average value of solar radiation was observed as 755 W m^{-2} by digital solar power meter with an accuracy of ± 10 W m^{-2}. The accuracy of all the measuring instruments is shown in Table 3. The maximum uncertainty obtained in the current study in calculating the collector efficiency from various tests was found to be 5.4%.

Results and discussion

All the recorded data were divided into several tests run by choosing 30-min interval in order to obtain a quasi-steady-state condition. The allowable variations in radiation intensity, inlet, outlet and ambient temperatures in each test interval are 25 W m^{-2}, 0.5, 0.6, and 0.8 °C, respectively, for satisfying the requirements of ASHRAE Standard 93-86. The flat-plate solar collector's performance was experimented with lower volume fraction of 0.01% and by varying flow rates from 1 to 3 lpm. In the morning, up to a certain time, the experimental curves are scattered due to the weak morning sunshine and hence the temperature rise in the collector will be minimum. Then during the peak sunny period, the scatter reduces gradually with time when the incident heat flux increases, thereby increasing the outlet collector temperature and ambient temperature. The experimental and theoretical results are exhibited in the figures and equations that describe the collector efficiency against a reduced temperature parameter $(T_i - T_a)/G_T$ for each volume flow rate. The experimental and theoretical data are fitted with linear trend line equations for studying the characteristic parameters of the flat-plate solar collector. Figure 6 represents the solar intensity, the collector outlet fluid temperature, the inlet fluid temperature of solar collector and the ambient temperature versus time for CeO_2/water nanofluid at 1 lpm recorded on April 21, 2016 which was one of the clear sunny days.

Water as working medium

Experiments were conducted with water and CeO_2/water nanofluids as working fluid in flat-plate solar collector from 9:00 to 16:00 h. Figures 7 and 8 represent the relationship between reduced temperature parameter and efficiency for each flow rates with respect to experimental and analytical results. The experimental data and analytical data are fitted with linear trend line equations for describing characteristic parameters such as the energy absorbed parameter $F_R(\tau\alpha)$ and the removed energy parameter $F_R U_L$ of flat-plate solar collector which are tabulated in Table 4. Absorbed energy parameter $F_R(\tau\alpha)$ is obtained by intersecting the trend line with y-axis, and the collector efficiency is maximum at this point. Energy removal factor $F_R U_L$ is calculated by the slope of trend line. Stagnation point also termed as zero efficiency is the intersection point of the trend line with the x-axis, and the situation happens when there is no fluid flow in the collector. It is observed from Table 4, Figs. 7 and 8 that the energy absorbed parameter $F_R(\tau\alpha)$ is maximum for the flat-plate solar collector at the flow rate of 3 lpm in both experimental and theoretical investigations, respectively. Hence according to Eq. (4), the maximum efficiency of the collector is 61.3% in the case experimental investigations and 65.9% in theoretical investigation with an error of ± 7.5%. When the flow rate is decreased from 3 lpm efficiency of the collector, there is decrease because of the decrement in heat capacity of the fluid and increase in temperature difference. This leads to higher heat losses, and there is an experimental and theoretical value corresponding to decrement in the useful energy gain. The

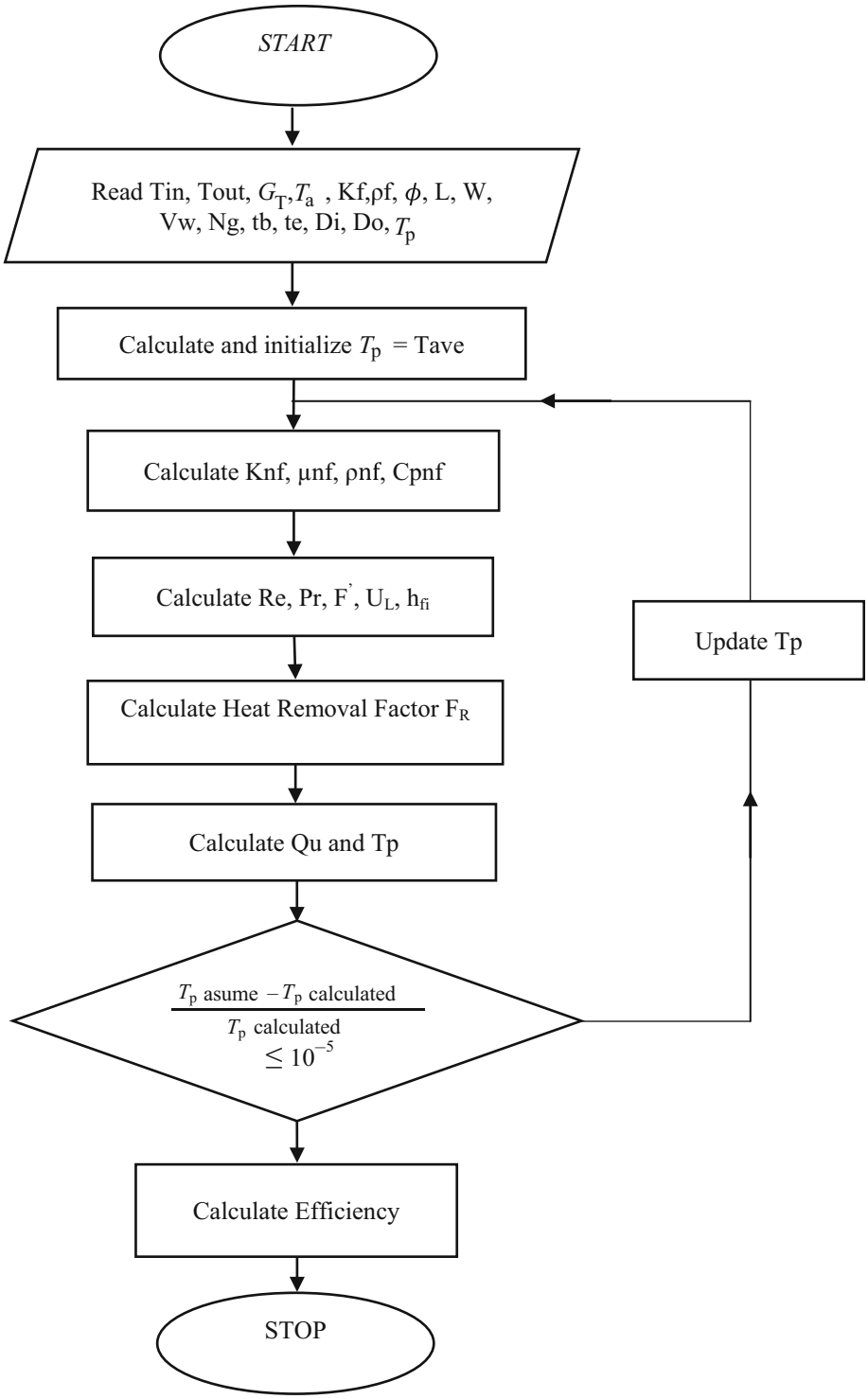

Fig. 4 Flow chart for MATLAB program

maximum energy removed parameter $F_R U_L$ for experimental and theoretical values for the flow rate of 3 lpm is 14.30 and 15.07, respectively. It is also observed that from Table 4 the maximum error percentage is about ± 7.5% when comparing both experimental and theoretical investigations.

Effect of working nanofluid for different flow rates

For any thermal system, efficiency is one of the most deciding parameter. For a flat-plate collector solar water heating system, the efficiency may be defined as the ratio of the output energy given by the solar collector to the

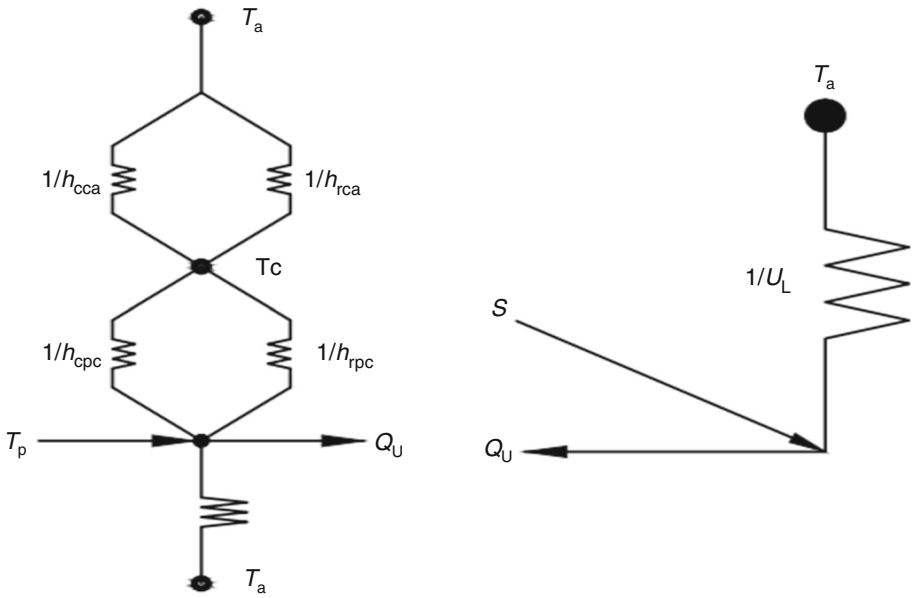

Fig. 5 Thermal network diagram for flat-plate collector

Table 3 Specifications of measuring instruments

Sl. no.	Instrument	Specification/range	Accuracy
1	Thermocouple	K-type/0–200 °C	± 0.5/ °C
2	Solar power meter	Class-A/ 0–2000 W m^{-2}	± 10/ W m^{-2}
3	Flow meter	0–10 LPM	± 2%
4	Anemometer	Cup type/0–15 m s^{-1}	± 0.2/m s^{-1}

input energy supplied by solar radiation. The efficiency is also determined by various other parameters like intensity of solar radiation falling on the collector, product of glazing's transmittance, type of nanofluid, particle size, volume concentration, inlet temperature of nanofluid, outside air temperature and absorbing plate's absorptance. Figures 9 and 10 show the variation of instantaneous collector efficiency versus reduced temperature parameter $(T_i - T_a)/G_T$ for CeO_2/water nanofluid with various volume flow rates representing experimental and theoretical analysis, respectively. The experimental and theoretical data which have all the flow rates are fitted with linear trend line equations for describing characteristic parameters of flat-plate solar collector. It is seen from the Figs. 9 and 10 that CeO_2/water nanofluid at the flow of 2 lpm gives maximum efficiency of 78.2% for experimental study whereas 76.7% in case of theoretical analysis. It is also

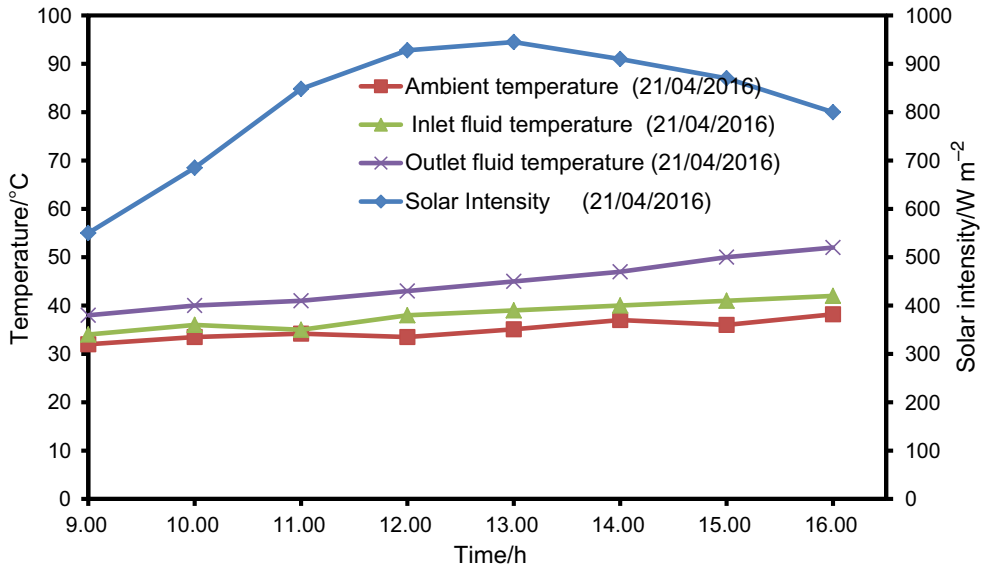

Fig. 6 Solar radiation, fluid inlet, outlet and atmosphere temperature

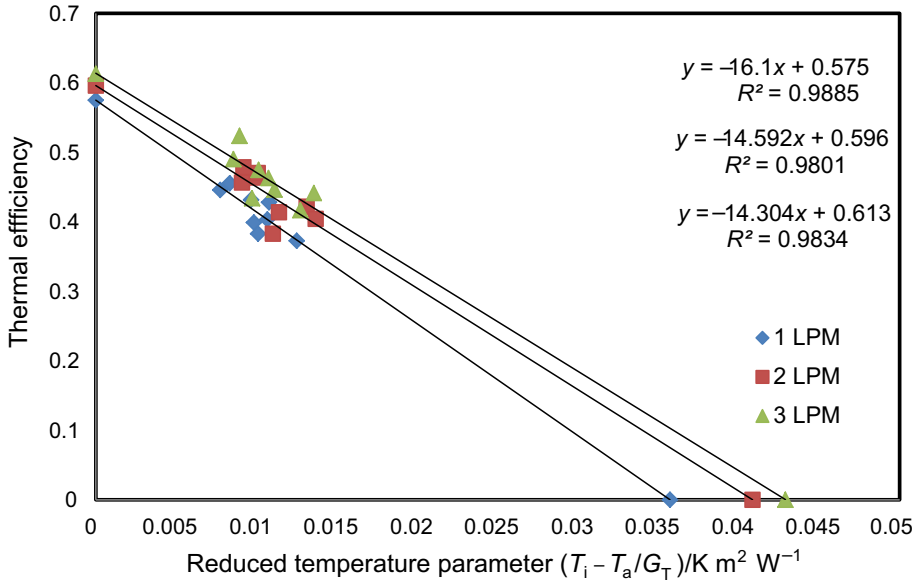

Fig. 7 Efficiency of the flat-plate collector with water as working fluid (Experimental)

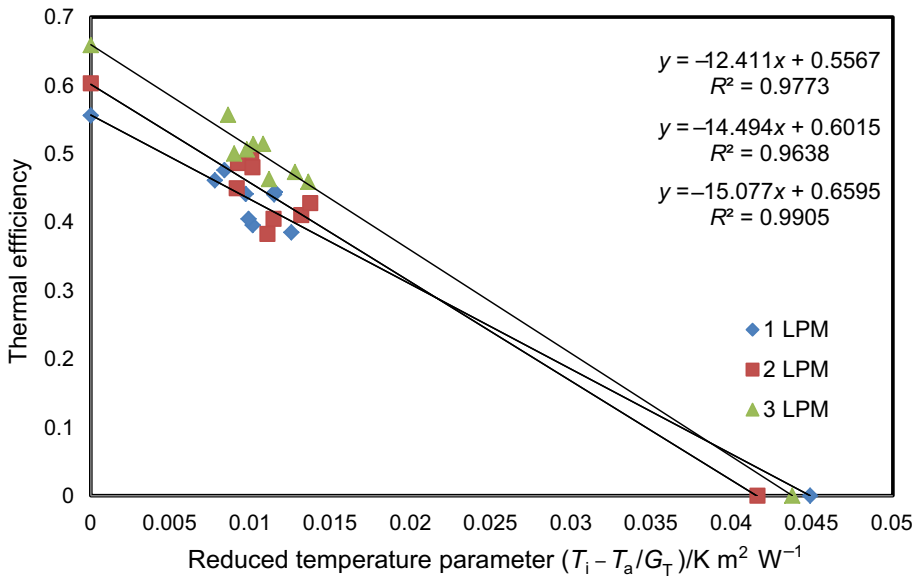

Fig. 8 Efficiency of the flat-plate collector with water as working fluid (Theoretical)

Table 4 Values of $F_R(\tau\alpha)$ and F_RU_L of the flat-plate collector at three flow rates with water as working fluid

Flow rate/lpm	F_RU_L			$F_R(\tau\alpha)$			R^2	
	Exp	Theo	Error %	Exp	Theo	Error %	Exp	Theo
1	14.1	13.41	− 5.1	0.575	0.556	− 3.3	0.990	0.977
2	14.59	14.49	− 0.68	0.596	0.601	0.83	0.976	0.963
3	14.30	15.07	5.38	0.613	0.659	7.5	0.990	0.990

observed that the trend lines with respect to 1 and 3 lpm intersect at reduced temperature parameter $(T_i - T_a)/G_T$ having a value of 0.018. The reason is that the operating of solar collector will not be that much effective when the reduced temperature parameter $(T_i - T_a)/G_T$ is greater than 0.018 in case of 3 lpm after which the efficiency of solar collector gets decreased when compared to 1 lpm flow rate. In case of theoretical analysis, the point of intersection of those trend lines was observed at 0.028 which is slightly higher. Figures 11–13 exhibit the effect of CeO_2/water

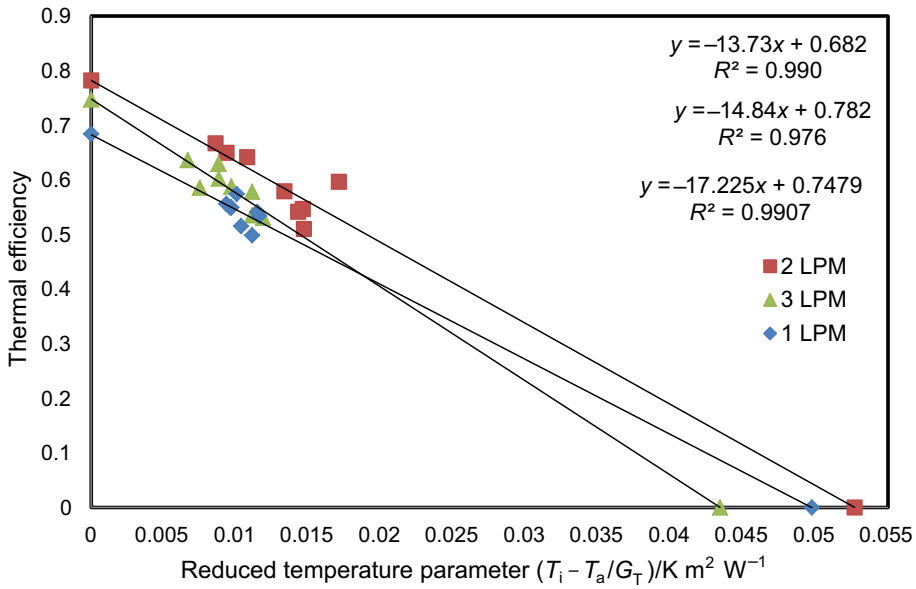

Fig. 9 Efficiency of CeO_2/water nanofluid (experimental)

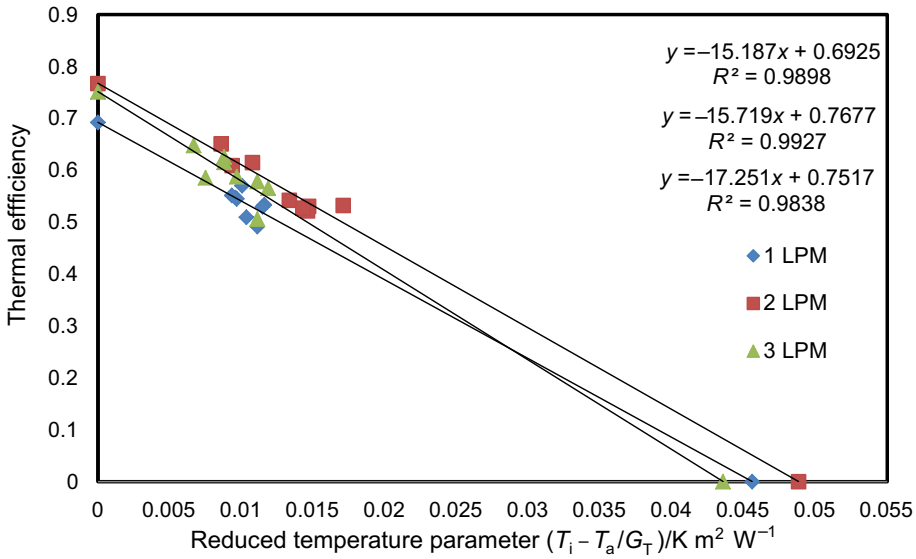

Fig. 10 Efficiency of CeO_2/water nanofluid (Theoretical)

nanofluid and water on the collector efficiency for 1, 2 and 3 lpm, respectively. It is seen that for all the selected flow rates, the collector efficiency using nanofluid is much higher than water as the base fluid. In the following Table 5, the collector efficiency parameters of both experimental and theoretical values of $F_R(\tau\alpha)$ and $F_R U_L$ have been tabulated for all the volume flow rates of working nanofluid. It is seen that the instantaneous collector efficiency for CeO_2/water nanofluid operating at 2 lpm is higher when compared with the efficiencies of the collector operating at other two flow rates. This can be deduced by comparing energy removal factor $F_R U_L$ and absorbed energy factor $F_R(\tau\alpha)$ of all the flow rates of nanofluids. It is observed that the efficiency of CeO_2/water nanofluid at 2 lpm is 21.5% higher than that of water as base fluid and 4.4% enhancement when compared with same working fluid with higher flow rate (3 lpm). It is interesting to see that when the flow rate is increased from 2 to 3 lpm, there is a gradual decrease in the efficiencies of the collector as given in Table 5. As per Eq. 4, the energy absorbed parameter $F_R(\tau\alpha)$ is dominant in the region of lower temperature differences and the removed energy parameter $F_R U_L$ is dominant in the region of higher temperature differences. At the flow rate of 2 lpm, the time of circulation of the nanofluids in the collector is higher and hence greater absorption of solar energy which leads to more temperature rise thereby higher heat transfer rate. At higher flow rates, the temperature rise in the fluid itself is small due to lesser residence time of nanofluids and hence lower heat transfer rate. It is also seen that collector

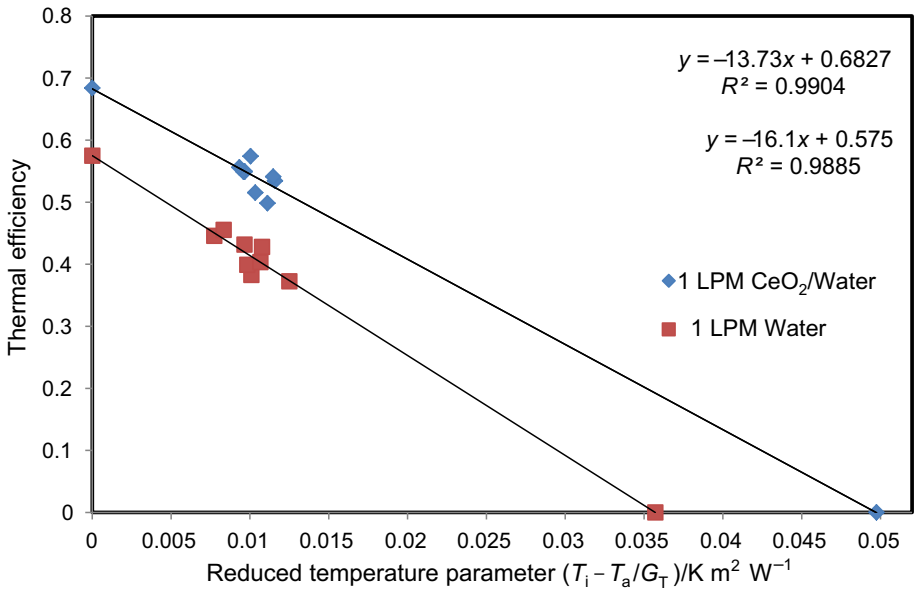

Fig. 11 Efficiency at 1 lpm flow rate for water and CeO_2/water nanofluid

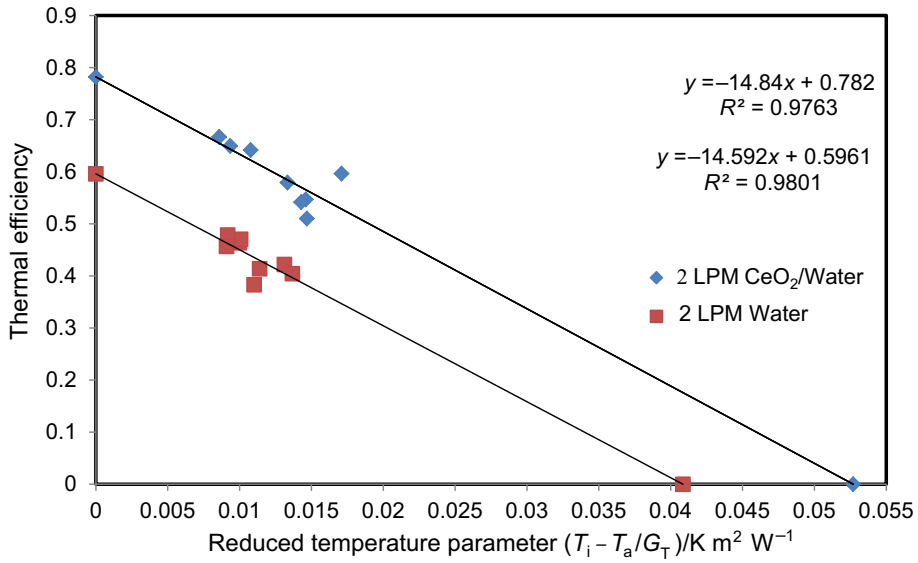

Fig. 12 Efficiency at 2 lpm flow rate for water and CeO_2/water nanofluid

efficiency increases with the increase in flow rate up to certain limit after which it shows negative results. The primary reason is Reynolds number increased with the increase in flow rate, thereby increasing the velocity and improvement in heat transfer coefficient. Beyond the certain limit, increased flow rate causes reduction in bulk temperature of the nanofluids and hence the reduced enhancement in thermal conductivity in the working fluids. Moreover, it is observed that CeO_2/water nanofluid with lower volume of 0.01% provided more stability and homogeneous mixture throughout the experimental investigation in the forced circulation study.

Heat transfer coefficient of any nanofluid depends on both the thermal properties of a base fluid, the hydrodynamic characteristics of its flow and its thermal boundary conditions. For CeO_2/water nanofluid with lower volume of 0.01%, a mathematical equation (Eq. 27) has been used for evaluating heat transfer coefficient for different volume flow rates and conditions. A graph has been plotted between heat transfer coefficient and time for various flow rates of working fluid, and it is exhibited in Fig. 14. It is observed from Fig. 14 that the heat transfer coefficient values are decreasing when the flow rate is increasing during laminar flow region. This is because when the flow rate increases the bulk mean temperature is decreased. Moreover, the thermal conductivity of the working fluid is directly proportional to mean temperature as per Eqs. 6 and 7. So when the thermal conductivity

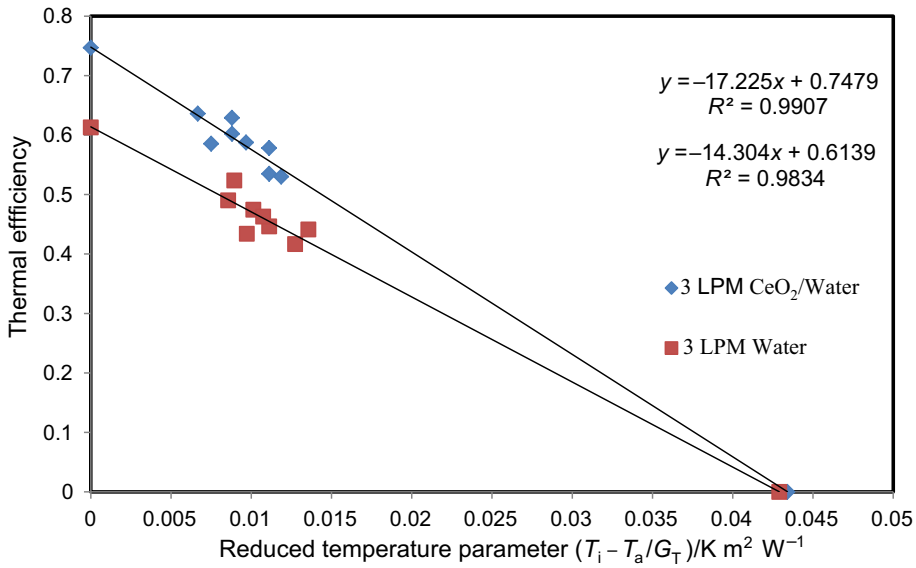

Fig. 13 Efficiency at 3 lpm flow rate for water and CeO_2/water nanofluid

Table 5 Values of $F_R(\tau\alpha)$ and $F_R U_L$ of the flat-plate collector at three flow rates with CeO_2/water working nanofluid

Flow rate/lpm	$F_R U_L$			$F_R(\tau\alpha)$			R^2	
	Exp	Theo	Error %	Exp	Theo	Error %	Exp	Theo
1	13.97	15.18	7.9	0.682	0.692	1.46	0.990	0.989
2	14.84	15.71	5.8	0.782	0.767	− 1.9	0.976	0.992
3	17.22	17.25	0.1	0.747	0.751	0.5	0.990	0.983

decreases heat transfer coefficient also decreased according to Eq. 27.

For predicting dimensionless outlet temperature (T_{out}/T_a) of the collector as a function of flow rate and reduced temperature $(T_i - T_a)/G_T$, a nonlinear regression software Lab fit has been used to develop a correlation. The regression analysis of the collector is shown in Fig. 15. The outlet temperature of solar collector is directly proportional to the density of the working fluid and inversely proportional to the specific heat capacity of the fluid. CeO_2/water nanofluid has a low specific heat capacity, thereby providing the greater value of outlet temperature. Not only specific heat capacity of the working fluid but also its density plays an important role that determines the outlet temperature of the collector. As CeO_2/water nanofluid has a higher density, it will have a lower flow velocity thereby it can absorb higher thermal energy and consequently the increased outlet temperature. The regression analysis gives the following equation to predict the non-dimensional outlet temperature as

$$T_{out}/T_a = 0.2192(T_i - T_a/G_T)^{(-0.02358+(-0.036577/Q)} + 0.3053Q \quad (33)$$

With a correlation coefficient value of $R^2 = 0.91$, the above equation can predict the outlet temperature with a possible error of 9.6%.

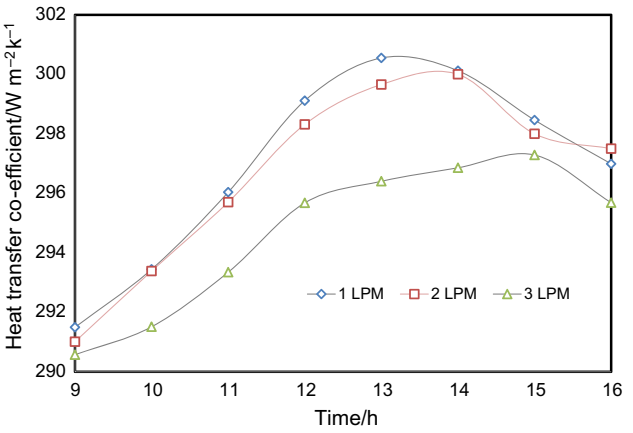

Fig. 14 Heat transfer coefficient at different flow rates for CeO_2/water nanofluids

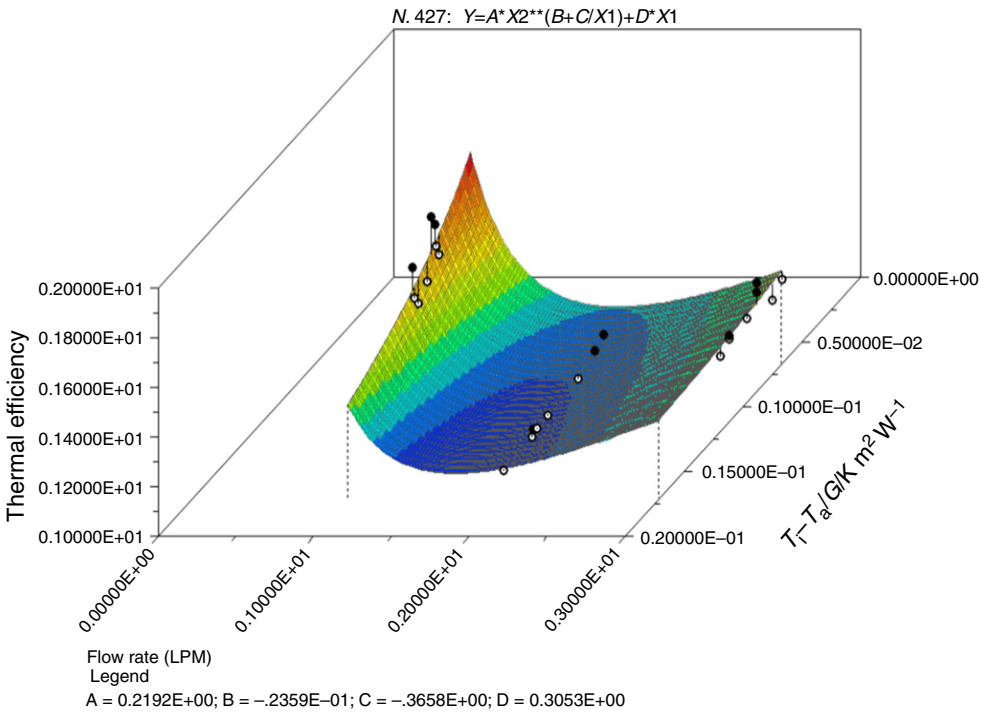

Fig. 15 Regression analysis

Energy and cost savings

When the solar collector is operated with CeO_2/water nanofluid, 25.2% of collector area can be reduced when compared with the collector area of conventional solar collector to obtain identical performance. Hence, it is seen that the nanofluid-based solar collector is 11.2% lower than the cost of water-operated solar collector due to reduction in collector area. It was also calculated that the conventional solar collector and CeO_2/water nanofluid-based solar collector consumes 882.8 and 626.8 MJ of embodied energy, respectively, due to which about 28.9% of embodied energy is saved when the solar collector is operated with CeO_2/water nanofluid.

Conclusions

The performance of flat-plate solar water heating system was experimentally analysed with CeO_2/water nanofluid as working fluid for lower volume concentration of 0.01% and by varying flow rate from 1 to 3 lpm. Also the performance of solar collector has been analysed theoretically using mathematical models for similar conditions. The results have been compared with the performance of water as base fluid both experimentally and theoretically. The enhancement in the efficiency of solar collector at 2 lpm was found to be 21.5% higher than that of water as base fluid in experimental investigation. The same enhancement was also observed during theoretical investigation with an error of ± 7.5%. It was again observed that the performance of solar collector using nanofluid is higher at all the flow rates when compared with water as base fluid. When the flow rate is increased from 2 to 3 lpm, the efficiency of the system was found to be 4.4% lower due to the thermal characteristics of the working fluid. During theoretical investigations, it was found that the heat transfer coefficient decreases with the increase in volume flow rate in laminar flow region. Correlation for predicting non-dimensional outlet temperature has also been developed using Lab fit software with a possible error of 9.6% for the performance of solar collector using CeO_2/water nanofluid having lower volume concentration of 0.01% in the current study.

References

1. Verma SK, Tiwari AK. Application of nanoparticles in solar collectors: a review. Mater Today Proc. 2015;2(4–5):3638–47.
2. Ferrouillat S, Bontemps A, Poncelet O, Soriano O, Gruss JA. Influence of nanoparticle shape factor on convective heat transfer and energetic performance of water-based SiO_2 and ZnO nanofluids. Appl Therm Eng. 2013;51:839–51.
3. Fuskele V, Sarviya RM. Recent developments in nanoparticles synthesis, preparation and stability of nanofluids. Mater Today Proc. 2017;4(2):4049–60.
4. Wong KV, De Leon O. Applications of nanofluids: current and future. Adv Mech Eng. 2010;2:519659.
5. Peyghambarzadeh SM, Hashemabadi SH, Naraki M, Vermahmoudi Y. Experimental study of overall heat transfer coefficient in the application of dilute nanofluids in the car radiator. Appl Therm Eng. 2013;52:8–16.

6. Kole M, Dey TK. Thermal performance of screen mesh wick heat pipes using water based copper nanofluids. Appl Therm Eng. 2013;50:763–70.
7. Srivastva U, Malhotra RK, Kaushik SC. Review of heat transport properties of solar heat transfer fluids. J Therm Anal Calorim 1–17.
8. Mu L, Zhu Q, Si L. Radiative properties of nanofluids and performance of a direct solar absorber using nanofluids. In: Proceedings of the 2nd ASME micro/nanoscale heat & mass transfer international conference, vol. 1; 2010. p. 549–53.
9. Jooa SH, Zhao D. Environmental dynamics of metal oxide nanoparticles in heterogeneous systems: a review. J Hazard Mater. 2017;322:29–47.
10. Zamzamian A, Keyanpour Rad M, Kiani Neyestani M, Jamal-Abad MT. An experimental study on the effect of Cu synthesized/EG nanofluid on the efficiency of flat-plate solar collectors. Renew Energy. 2014;71:658–64.
11. Michael JJ, Iniyan S. Performance of copper oxide/water nanofluid in a flat plate solar water heater under natural and forced circulations. Energy Convers Manag. 2015;95:160–9.
12. Moghadam AJ, Farzane-Gord M, Sajadi M, Hoseyn-Zadeh M. Effects of CuO/water nanofluid on the efficiency of a flat-plate solar collector. Exp Therm Fluid Sci. 2014;58:9–14.
13. He Q, Zeng S, Wang S. Experimental investigation on the efficiency of flat-plate solar collectors with nanofluids. Appl Therm Eng. 2014;53:1–7.
14. Menbari A, Alemrajabi AA, Rezaei A. Heat transfer analysis and the effect of CuO/Water nanofluid on direct absorption concentrating solar collector. Appl Therm Eng. 2016;104:176–83.
15. Tooraj Y, Farzad V, Ehsan S, Sirus Z. An experimental investigation on the effect of Al_2O_3–H_2O nanofluid on the efficiency of flat-plate solar collectors. Renew Energy. 2012;39:293–8.
16. Gangadevi R, Senthilraja S, Imam SA. Efficiency analysis of flat plate solar collector using Al_2O_3–water nanofluid. Ind Streams Res J. 2013;3:1–4.
17. Raei B, Shahraki F, Jamialahmadi M, Peyghambarzadeh SM. Experimental study on the heat transfer and flow properties of γ-Al_2O_3/water nanofluid in a double-tube heat exchanger. J Therm Anal Calorim. 2017;127:2561–75.
18. Gupta HK, Agrawal GD, Mathur J. Investigations for effect of Al_2O_3–H_2O nanofluid flow rate on the efficiency of direct absorption solar collector. Case Stud Thermal Eng. 2015;5:70–8.
19. Colangelo G, Favale E, Miglietta P, de Risi A, Milanese M, Laforgia D. Experimental test of an innovative high concentration nanofluid solar Collector. Appl Energy. 2015;154:874–81.
20. Mahian O, Kianifar A, Sahin AZ, Wongwises S. Entropy generation during Al_2O_3/water nanofluid flow in a solar collector: effects of tube roughness, nanoparticle size, and different thermophysical models. Int J Heat Mass Transfer. 2014;78:64–75.
21. Verma SK, Tiwari AK, Chauhan DS. Performance augmentation in flat plate solar collector using MgO/water nanofluid. Energy Convers Manag. 2016;124:607–17.
22. Meibodi SS, Kianifar A, Mahian O, Wongwises S. Second law analysis of a nanofluid-based solar collector using experimental data. J Therm Anal Calorim. 2016;126:617–25.
23. Anin Vincely D, Natarajan E. Experimental investigation of the solar FPC performance using graphene oxide nanofluid under forced circulation. Energy Convers Manag. 2016;117:1–11.
24. Karami M, Akhavan-Bahabadi MA, Delfani S, Ghozatloo A. A new application of carbon nanotubes nanofluid as working fluid of low-temperature direct absorption solar collector. Sol Energy Mater Sol Cells. 2014;121:114–8.
25. Natarajan E, Sathish R. Role of nanofluids in solar water heater. Int J Adv Manuf Technol. 2009. https://doi.org/10.1007/S00170-008-1876-8.
26. Estellé P, Halelfadl S, Maré T. Thermophysical properties and heat transfer performance of carbon nanotubes water-based nanofluids. J Therm Anal Calorim. 2017;127(3):2075–87.
27. Delfani S, Karami M, Akhavan-Behabadi MA. Performance characteristics of a residential type direct absorption solar collector using MWCNT nanofluid. Renew Energy. 2016;87:754–64.
28. Pandey AK, Tyagi VV, Rahim NA, Kaushik SC, Tyagi SK. Thermal performance evaluation of direct flow solar water heating system using exergetic approach. J Therm Anal Calorim. 2015;121:1365–73.
29. Saidur R, Meng TC, Said Z, Hasanuzzaman M, Kamyar A. Evaluation of the effect of nanofluid-based absorbers on direct solar collector. Int J Heat Mass Transfer. 2012;55:5899–907.
30. Buongiorno J. Convective transport in nanofluids. J Heat Transfer. 2005;128(3):240–50.
31. Faizal M, Saidur R, Mekhilef S, Alim MA. Energy, economic and environmental analysis of metal oxides nanofluid for flat-plate solar collector. Energy Convers Manag. 2013;76:162–8.
32. Todd Otanicar P, Jay GS. Comparative environmental and economic analysis of conventional and nanofluid solar hot water technologies. Environ Sci Technol. 2009;43(15):6082–7.
33. Hama J, Kima J, Cho H. Theoretical analysis of thermal performance in a plate type liquid heat exchanger using various nanofluids based on Libr solution. Appl Therm Eng. 2016;108:1020–32.
34. Ko YG, Do T, Chun Y, Kim CH, Choi US, Kim JY. CeO_2-covered nanofiber for highly efficient removal of phosphorus from aqueous solution. J Hazard Mater. 2016;307:91–8.
35. Liying HE, Jumin SU, Lanhong J, Shikao SHI. Recent advances of cerium oxide nanoparticle synthesis. Luminescence and biomedical studies: a review. J Rare Earths. 2015;33:791–9.
36. Otanicar T, Phelan PE, Prasher RS, Rosengarten G, Taylor RA. Nanofluid-based direct absorption solar collector. J Renew Sustain Energy. 2010;2:033102.
37. Xuan Y, Li Q, Hu W. Aggregation structure and thermal conductivity of nanofluids. AIChE J. 2003;49:1038–43.
38. Nieto de Castro CA, Li SFY, Nagashima A, Trengove RD, Wakeham A. Standard reference data for the thermal conductivity of liquids. J Phys Chem Ref Data. 1986;15:1073–86.
39. Corcione M. Empirical correlating equations for predicting the effective thermal conductivity and dynamic viscosity of nanofluids. Energy Convers Manag. 2011;52:789–93.
40. Khanafer K, Vafai K. A critical synthesis of thermophysical characteristics of nanofluids. Int J Heat Mass Transfer. 2011;54:4410–28.
41. Duffie JA, Beckman WA. Solar engineering of thermal processes. 3rd ed. New York: Wiley; 2006.
42. Kalogirou SA. Solar energy engineering: processes and systems. 2nd ed. Oxford: Elsevier; 2013.